High speed PIV of flame propagation in obstructed channels

T. Li, R. P. Lindstedt[1]
Department of Mechanical Engineering, Imperial College, Exhibition Road,
London SW7 2AZ, UK

Abstract Turbulence-chemistry interactions and fuel (or mixture) reactivity directly affect flame acceleration caused by positive feedback mechanisms in obstacles laden channels. The use of more reactive hydrogen enriched fuels is increasingly important due to the desire to use syngas and/or biogas in power generation applications. However, experimental data remains limited due to difficulties in achieving repeatable results. The current study reports highly reproducible experiments performed using strongly hydrogen enriched fuel lean CH_4/H_2/air mixtures with the flame propagation leading up to a turbulent explosion quantified using high-speed particle image velocimetry (HS-PIV) and Mie scattering. The time-resolved evolution of the recirculation zone was successfully captured with the explosion over-pressure and flame propagation speed also measured. A peak over-pressure of 37 kPa and a flame speed of 190 m/s were obtained. The horizontal and vertical velocity components were calculated at selected spatial locations in the free flow, shear layer and recirculation zone. In the free flow region, $\bar{u}$ is dominant, while in shear layer $\bar{u}$ and $\bar{v}$ are comparable with the thickness of the shear layer was estimated to be 10 mm based on the velocity gradient. The change in the horizontal velocity against height is also reported. It is expected that the data will be useful in risk assessments of explosion hazards and for model development.

1 Introduction

The positive feedback mechanism caused by obstacles in the flame path is well established and has been the subject of extensive investigations e.g. [1–10]. The studies have covered a broad range of influential factors, such as the blockage ratio, obstruction type and obstacle separation distance, under conditions that may lead to a deflagration to detonation transition (DDT) through continuous flame acceleration. Cross and Ciccarelli [11] recently studied the flame propagation in an obstacle-filled tube, suggesting that shock reflection plays an critical role in the quasi-detonation regime. The strong turbulence generated in recirculation zones behind obstacles is a key feature of the flame acceleration process leading up quasi-detonations. Lindstedt and Sakthitharan [12] provided an insightful quantitive description of the flow field development in a flame tube fitted with a baffle-type obstacle using laser doppler anemometry (LDA) and stoichiometric methane-air mixtures. The rates of production and dissipation of turbulence were also estimated and it was concluded that the flow field in the recirculation zone was highly turbulent. Anisotropy was observed in the shear layer above the obstacle. Hampp and Lindstedt [13] performed 10 kHz PIV measurements in the recirculation region behind a single obstacle with a turbulence-generating cross fractal grid (CFG) installed upstream of the obstacle (between the obstacle and ignition spark). The impact of different CFGs was investigated with the flame passing through the CFG visualised using chemiluminescence based imaging at 2.5 kHz. Boeck et al. [14] performed simultaneous OH-PLIF and schlieren measurements on flame

[1]Corresponding author: p.lindstedt@imperial.ac.uk

acceleration in an obstacle-laden channel with the interactions between shock and flame analysed in detail. Numerical simulations were also performed [15]. Li et al. [16] measured the over-pressures generated in a flame tube for a wide range of hydrogen enriched CO and CH_4 mixtures. Two obstacles were installed in a staggered arrangement with flame propagation speeds also obtained using ionisation probes. The data was used to explore the relationship between the mixture composition and the resulting peak over-pressure. A proposed scaling parameter (β) was found to be very useful in correlating the results.

The current CH_4/H_2/air mixture was selected based on the previous study [16] and has a hydrogen content of 80% and an equivalence ratio of 0.60. The fuel lean mixture was chosen due to the relevance to power generation using gas turbines and gas engines. In previous work [13], the measurement window was located 50 mm downstream the obstacle (the height of the obstacle was 36 mm) and it is essential to develop a better understanding of the flow field close to the obstacle. The current measurement window accordingly starts 3 mm downstream. The geometry was also simplified by the replacement of the cross-fractal grid with a solid obstacle to more readily facilitate theoretical studies.

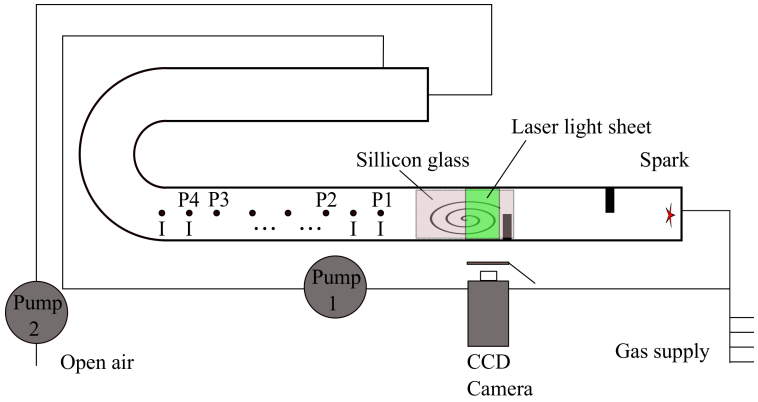

Figure 1: Schematic of the experimental facility.

2 Experimental setup

The experiments were performed in a flame tube facility, see Fig. 1, consisting of an optical, a driven and an end sections. The optical and driven sections have a rectangular cross-section of 34 $\times$ 72 mm and the end section a round cross-section of 80 mm inside diameter. The latter was used to provide a longer test time free of reflected pressure waves from the closed end section. Two solid obstacles with a thickness of 5 mm and a height of 36 mm (blockage ratio of 50%) were installed at distances of 80 mm and 400 mm from the ignition end in a staggered arrangement. A standard electronic ignition device (Sparkrite SX1000, EDA Sparkrite, Ltd.) was installed at the upstream end. Eight ionisation probes were mounted along the tube and served as flame arrival time detectors. The pressure was measured using four piezo-electric pressure transducers (1 $\times$ PCB 113A21 and 3 $\times$ PCB 113B21; PCB Piezotronics, Inc.). A 12-bit data acquisition card (PCI-6115; National Instruments) with a recording rate of 1 MHz was used for the pressure transducers. The positions are specified in Table 1.

Table 1: Locations (X) of pressure transducers (P) and ionisation probe (I) detectors from the ignition end.

X [m]	0.845	1.075	1.305	1.535	2.000	2.225	3.145	3.450
Sensor	P1+I	I	P2+I	I	I	P3+I	P4+I	I

A high speed particle image velocimetry (HS-PIV) setup, controlled by LaVision Davis HS 8.3, was used to obtain flow velocities in the shear layer and the recirculation zone behind the second obstacle. The system, consisting of an Edgewave INNOSLAB Nd:YAG laser and a Photron Fastcam SA6, was timed and synchronised by an external LaVision HS controller. The camera was equipped with a 50 mm Nikon camera lens (f1.4) with a mounted 3 nm narrow bandwidth filter for a wavelength of 532 nm. The field of view was set to 84.0 mm $\times$ 71.0 mm as indicated by the green rectangle in Fig. 1. A convergent vertical laser light sheet with a thickness around 0.8 mm in the centre of the recirculation zone was introduced from the top of the optical section. The silicon oil seeding (droplet size $\leq$ 1.5 μm) was introduced along with the reactant mixture. The recording rate was set to 10 kHz at a resolution of 576 $\times$ 480 pixels. The timing between the double laser pulses was found to be optimum at Δt = 15 μs and background subtractions performed to enhance the signal to noise ratio prior to the calculation of the velocity vectors.

Before each experiment, the flame tube was flushed with air and evacuated to a pressure below 0.5 kPa. A partial pressure method, using a static pressure transducer (UNIK 5000; GE Measurement & Control), was applied to control the required proportions of the fuel/air mixture with the equivalence ratio controlled to $\Phi = 0.60 \pm 0.02$. The fuel purities were 99.5% (CH_4) and 99.99% (H_2). Mixture homogeneity was achieved by flow circulation using a diaphragm pump for 10 min corresponding to 23 tube-volumes. The mixture was left to settle to achieve quiescent conditions before ignition at an initial pressure of 50 kPa. The leak rate was $<$ 16 Pa/s with the total filling time less than 45 s. All data acquisition devices were triggered using the spark TTL signal to achieve synchronisation.

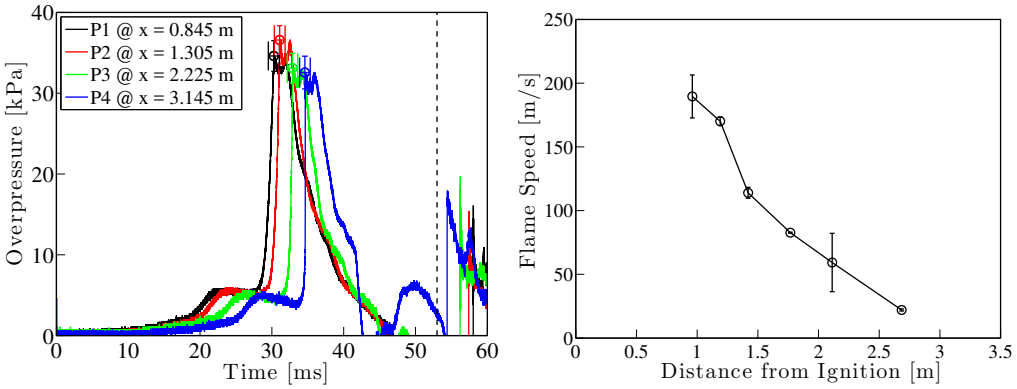

(a) Pressure development (b) Flame speeds

Figure 2: Pressure development and flame speeds.

3 Results and discussion

The pressure development and the corresponding flame speed are shown in Fig. 2. The peak over-pressure occurs at around 30 ms and results form the turbulent explosion behind the obstacle. The four lines correspond to the four pressure transducer locations given in Table 1. The highest over-pressure of 36.6 $\pm$ 1.8 kPa is reached at 31.1 $\pm$ 0.8 ms after ignition at location P2. The error bars were calculated based on four runs and indicate good repeatability both in terms of the peak pressure and the time evolution. The dashed line represents the arrival of the pressure back-reflection from the downstream closed end of the flame tube. The recorded flame propagation speed reaches a maximum around 190 m/s at a distance of 0.96 m and decreases continuously with distance along the tube – consistent with a decaying explosion.

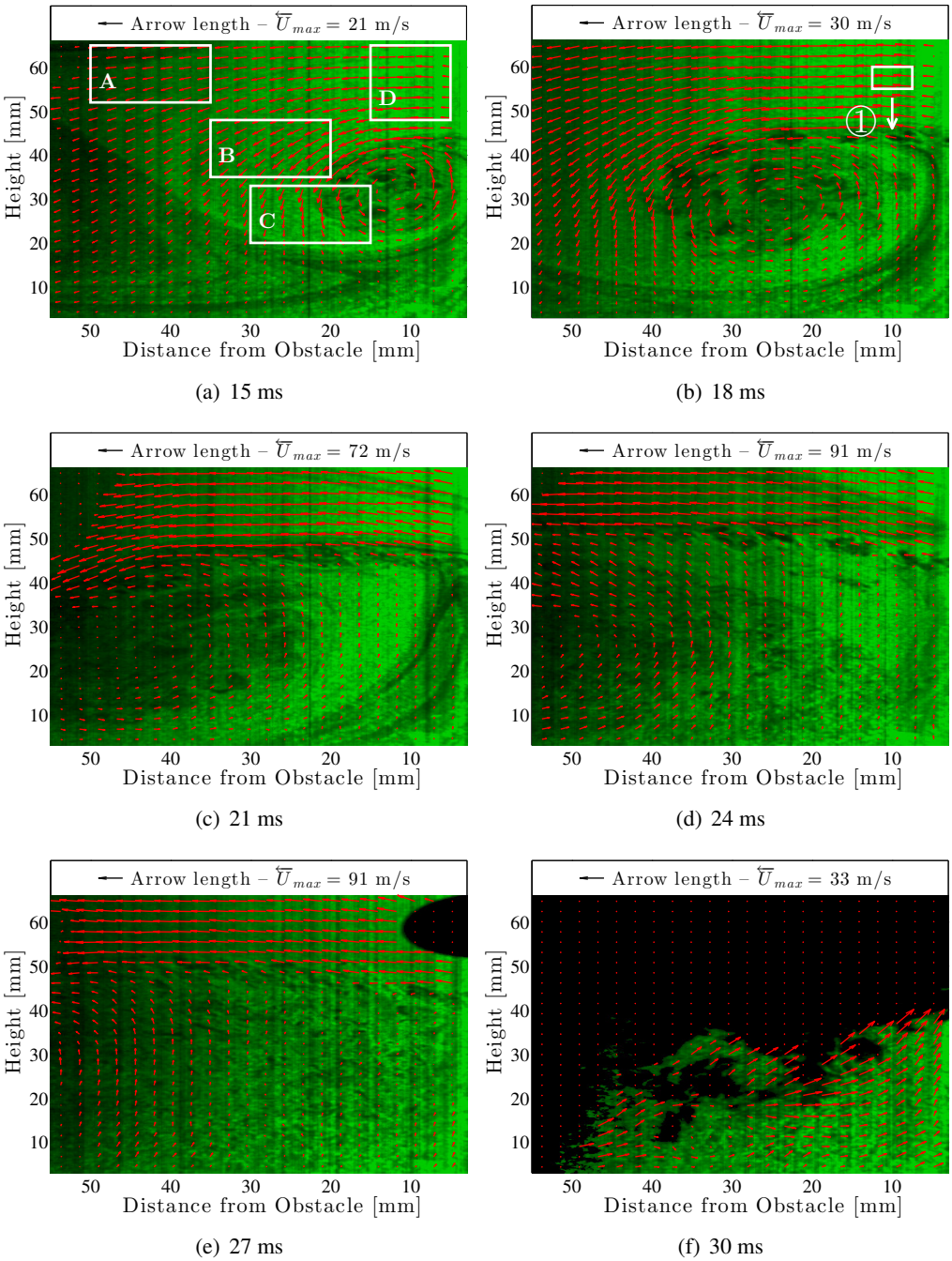

(a) 15 ms (b) 18 ms

(c) 21 ms (d) 24 ms

(e) 27 ms (f) 30 ms

Figure 3: Time series obtained using 10 kHz high speed Mie scattering with superimposed velocity vectors. The velocity vector length is scaled linearly with the magnitude and the reference given at the top of each sub-graph.

High speed PIV at 10 KHz was performed to better understand the evolution of the explosion in the critical part of the recirculation zone behind the obstacle. The PIV velocity vectors are shown superimposed on the Mie scattering images in Fig. 3. In the time window from 15 ms to 24 ms after ignition, the eddy continues

to grow with the centre gradually moving downstream away from the obstacle. The flame front, the black area in the top right hand corner of Fig. 3(e), arrived at 27 ms. A maximum velocity around 90 m/s was observed. The fuel in the recirculation zone is subsequently rapidly consumed via a highly fragmented flame front, as shown in Fig. 3(f), with islands of combustion products surrounded by reactants. The peak pressure also occurs at around this time (30 ms) showing that the turbulent explosion is a direct consequence of the fast fuel consumption in the recirculation zone behind the obstacle.

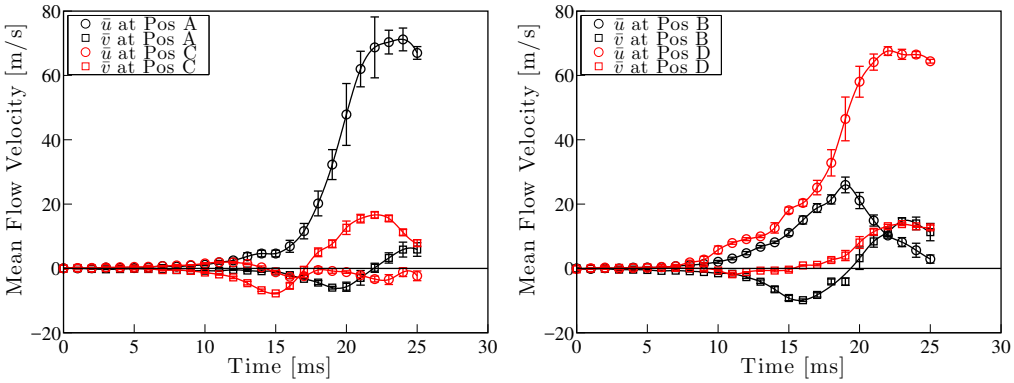

(a) $\bar{u}$ and $\bar{v}$ in window A and C

(b) $\bar{u}$ and $\bar{v}$ in window B and D

Figure 4: Mean horizontal ($\bar{u}$) and vertical ($\bar{v}$) velocity component in reference windows.

The mean velocity components in the horizontal ($\bar{u}$) and vertical ($\bar{v}$) directions were determined, see Fig. 4, for the set of window locations shown in Fig. 3(a). Windows A, B and C share a size of 15 $\times$ 13 mm (L $\times$ H) with centres (distances from (1) the obstacle, (2) the lower wall) at (42.5, 58.5 mm), (7.5, 41.5 mm) and (22.5, 26.5 mm), respectively. Window D has a size of 10 $\times$ 17 mm, centred at (10, 56.5 mm). Window A represents the free flow and the (horizontal) $\bar{u}$ component is dominant, while $|\bar{v}|$ is less than 10 m/s. In window B, where the shear layer is located, $\bar{u}$ and $\bar{v}$ are comparable. The $\bar{v}$ component increased after 10 ms and changed from negative to positive as a result of the downstream movement of the recirculation zone. In the region above the shear layer (window D), $\bar{u}$ is also dominant. In both windows A and D, the $\bar{v}$ component has a minor impact on the velocity magnitude. The mean horizontal velocity component ($\bar{u}$) is shown in Fig. 5 for a 5 $\times$ 5 mm window shifted along a vertical line located 10 mm downstream of the obstacle, see Fig. 3(b). The dashed line indicates the height of the obstacle with $\bar{u}$ negative because of the recirculating flow. The velocity increases sharply in the shear layer until a peak is reached around 50 mm (14 mm above the obstacle), suggesting a thickness of the shear layer around 10 mm according to the vertical gradient of $\bar{u}$. Above the shear layer, $\bar{u}$ exhibits a minor decrease as the height increases due to the friction at the top wall. The maximum velocity also increases with the time after ignition as a result of the flame acceleration.

4 Conclusions

The current HS-PIV measurements are part of a comprehensive data set providing quantification of the flow field evolution in the recirculation zone ahead of an advancing flame front. The Mie scattering images further illustrate the fragmented flame structure during the highly turbulent explosion phase. The horizontal and vertical velocity components were calculated in the free flow, shear layer, recirculation zone and the region

above the obstacle. In the free flow region, $\bar{u}$ is dominant while in shear layer, $\bar{u}$ and $\bar{v}$ are comparable. The change of the horizontal velocity against height was also determined along with the over-pressure and flame arrival times. The data sets are expected to be helpful in understanding the temporal evolution of high speed explosions and thereby support the development of improved tools for the quantitative risk assessments.

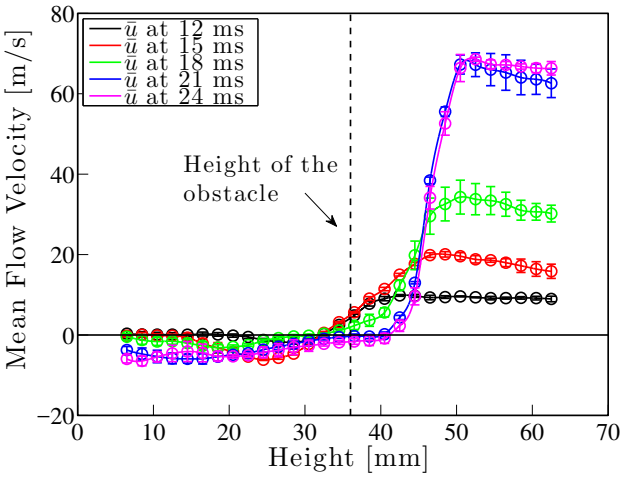

Figure 5: Horizontal ($\bar{u}$) velocity along a vertical line 10 mm downstream the second obstacle as indicated in Fig. 3(b).

Acknowledgements

The authors gratefully acknowledge the support of the ETI under the High Hydrogen project (PE02162) for the construction of some aspects the experimental facility. Discussions with Dr Fabian Hampp are also gratefully acknowledged along with the financial support of the China Scholarship Council for Mr Tao Li.

References

[1] I. O. Moen, M. Donato, R. Knystautas, and J. H. Lee. *Combust. Flame*, 39(1):21–32, 1980.
[2] R. P. Lindstedt and H. J. Michels. *Combust. Flame*, 76(2):169–181, 1989.
[3] S. S. Ibrahim and A. R. Masri. *J. Loss Prevent. Proc.*, 14(3):213–221, 2001.
[4] A. M. Na'inna, H. N. Phylaktou, and G. E. Andrews. *J. Loss Prevent. Proc.*, 26(6):1597–1603, 2013.
[5] V. N. Gamezo, T. Ogawa, and E. S. Oran. *Combust. Flame*, 155(1-2):302–315, 2008.
[6] D. Bradley, M. Lawes, and K. Liu. *Combust. Flame*, 154(1-2):96–108, 2008.
[7] G. Ciccarelli, C. T. Johansen, and M. Parravani. *Combust. Flame*, 157(11):2125–2136, 2010.
[8] B. J. Lowesmith, C. Mumby, G. Hankinson, and J. S. Puttock. *Int. J. Hydrogen Energ.*, 36(3):2337–2343, 2011.
[9] T. Ogawa, V. N. Gamezo, and E. S. Oran. *J. Loss Prevent. Proc.*, 26(2):355–362, 2013.
[10] C. Chan, I. O. Moen, and J. H. S. Lee. *Combust. Flame*, 49(1-3):27–39, 1983.
[11] M. Cross and G. Ciccarelli. *J. Loss Prevent. Proc.*, 36:380–386, 2015.
[12] R. P. Lindstedt and V. Sakthitharan. *Combust. Flame*, 114(3-4):469–483, 1998.
[13] F. Hampp and R. P. Lindstedt. CISM vol. 568, Springer-Verlag, pp. 75-102, 2016.
[14] L. R. Boeck, M. Kellenberger, G. Rainsford, and G. Ciccarelli. *Proc. Combust. Inst.*, 2016 (in press).
[15] L. R. Boeck, S. Lapointe, J. Melguizo-Gavilanes, and G. Ciccarelli. *Proc. Combust. Inst.*, 2016 (in press).
[16] T. Li, F. Hampp, and R. P. Lindstedt. In *25th ICDERS*, Leeds, UK, 2015.